# RESISTANCE SPOT WELDING OF ULTRA HIGH STRENGTH STEEL SHEETS WITH ALUMINUM MATERIALS

# ULTRA YÜSEK DAYANIMLI ÇELİK SACLARIN ALÜMİNYUM MALZEMELERLE DİRENÇ NOKTA KAYNAĞI

**BÜŞRA ODABAŞI ATAK**

**Asst. Prof. MEHMET OKAN GÖRTAN**
**Supervisor**

Submitted to
Graduate School of Science and Engineering of Hacettepe University
as a Fulfillment to the Requirements
for the Award of the Degree of Master of Science
in Mechanical Engineering

2023

# ABSTRACT

## RESISTANCE SPOT WELDING OF ULTRA HIGH STRENGTH STEEL SHEETS WITH ALUMINUM MATERIALS

**Büşra ODABAŞI ATAK**

This thesis aims to examine the joining of steel sheets with a yield strength of up to 1500MPa and aluminum materials by using resistance spot welding (RSW). Effect of electrode geometry and its combinations on the quality of the joint is investigated. Materials used are steel MS1500 and aluminum EN AW-6061-T6. Samples were produced, and iterations were observed on these samples to achieve the optimum combination in terms of mechanical strength by changing parameters such as current, time, and electrode type. The study was carried out on a scale between 11-14kA as current. The force was kept constant in all samples by taking 3kN. Welding times of 10 and 20 cycles were tested. Microstructure analysis, macrostructure analysis, and tensile-shear testing methods were applied to observe the results and achieve the goal of maximizing mechanical strength.. The macrostructure analysis examined the nugget diameter, melted zone geometry, joint geometry, and fracture type. Failure types were determined due to the tensile-shear test. Vickers hardness test was applied to specify the hardness of the joint.

**Keywords:** Resistance Spot Welding, RSW, Steel, Aluminum, MS1500, 6061

# ÖZET

## ULTRA YÜKSEK DAYANIMLI ÇELİK SACLARIN ALÜMİNYUM MALZEMELERLE DİRENÇ NOKTA KAYNAĞI

**Büşra ODABAŞI ATAK**

**Yüksek Lisans, Makina Mühendisliği Bölümü**
**Tez Danışmanı: Dr. Öğr. Üyesi Mehmet Okan GÖRTAN**
**Ocak 2023, 63 sayfa**

Bu tez, çekme dayanımı 1500MPa ve üzerinde olan çelik sacların ve alüminyum malzemelerle direnç nokta kaynağı kullanılarak birleştirilmesini incelemeyi amaçlamaktadır. Elektrod geometrisi kombinasyonlarının bağlantıların kalitesine etkisinin incelenmesi hedeflenmiştir. Kullanılan malzemeler çelik MS1500 ve alüminyum EN AW-6061-T6'dır. Optimum kombinasyonun elde edilmesi için numuneler üretilmiş ve bu numuneler üzerinde akım, zaman, elektrot gibi parametreler değiştirilerek mekanik dayanım açısından iterasyonlar gözlemlenmiştir. 11-14kA akım değerleri arasında bir ölçekte çalışma yapılmıştır. Kuvvet 3kN alınarak tüm numunelerde sabit tutulmuştur. 10 ve 20 çevrim kaynak süreleri denenmiştir.. Uygulanan parametre analizinin etkilerini gözlemlemek ve mekanik mukavemeti en üst düzeye çıkarma hedefine ulaşmak için mikro yapı analizi, makro yapı analizi, çekme-makaslama testi yöntemleri uygulanmıştır. Mikro yapı analizinde numuneler arasındaki farklılıklar gözlemlenmiştir. Çekirdek çapı, birleşim yeri, ısı tesiri altındaki bölgenin geometrisi ve kırılma tipi makro yapı analizlerinde incelenmiştir. Kırılma tipleri çekme testinde

belirlenmiştir. Birleşim yerinin sertliğinin belirlenmesi için Vickers sertlik testi uygulanmıştır.

**Anahtar Kelimeler:** Direnç Nokta Kaynağı, Çelik, Alüminyum, MS1500, 6061

# ACKNOWLEDGEMENTS

# TABLE OF CONTENTS

# LIST OF FIGURES

# LIST OF TABLES

# ABBREVIATIONS

| | |
|---|---|
| Al | Aluminum |
| BM | Base Metal |
| EBSD | Electron Back-Scattered Diffraction |
| FZ | Fusion Zone |
| HAZ | Heat Affected Zone |
| IMC | Intermetallic Compound |

# 1. INTRODUCTION

Researchers have turned to different materials and alternative production techniques in order to achieve great strength at low weights. Joining methods are constantly changing and evolving. Especially in the automotive industry, thinner materials with high strength are observed. The increase in the types of materials used in today's industry, the necessity of different metal connections in places that require different properties, and the importance of economic factors, especially in recent years, necessitate the use of materials with different properties.

Resistance spot welding is a method used to weld different metals together. This method creates high temperatures using electrical resistance to weld metal parts together. Its advantages are no filler material, high production rates, suitability for mechanization and automation, lower operator skill level, and good repeatability and reliability. At the same time, its disadvantages are high initial equipment cost and limited to lap joints for most resistance spot welding processes.

In the current study, effect of electrode geometry combinations on the quality of resistance spot welded joints of dissimilar materials. An ultra-high strength steel MS1500 and a high strength aluminium alloy EN AW-6061-T6 has been used.

# 2. LITERATURE SURVEY

## 2.1. Resistance Spot Welding

The problems experienced in the welding of thin metal materials and dissimilar materials used in many fields, such as the automotive industry, space, and aircraft technologies, have provided the development of different types of welding. Excessive plastic deformation is created in the thin-section materials when exposed to high temperatures. Also, it is difficult to establish bonds between two different types of materials, and it might cause metallurgical incompatibility. Therefore, it is necessary to perform the welding process at a minimum temperature and in the shortest time.

RSW is preferred for welding dissimilar materials and thin metal materials as it is a short and controllable manufacturing process. The main advantages of RSW are its cost and time-effectiveness. It is the welding operation that occurs with heat generated by the resistance of workpieces against electric current, and pressure created by electrodes used. The current and time are chosen according to the thickness of the parts. Then, sheets are placed appropriately between the electrodes. The upper electrode goes down towards the bottom. Workpieces are fixed by force between the lower and upper electrodes. The pressure is increased, and the passage of the electric current starts. The current transition heats the parts and starts melting. The current is cut off automatically, and workpieces are left to cool without removing the electrode pressure. After the weld pool is completely solidified, electrode pressure is removed [1]. RSW process is shown in Figure 1 schematically.
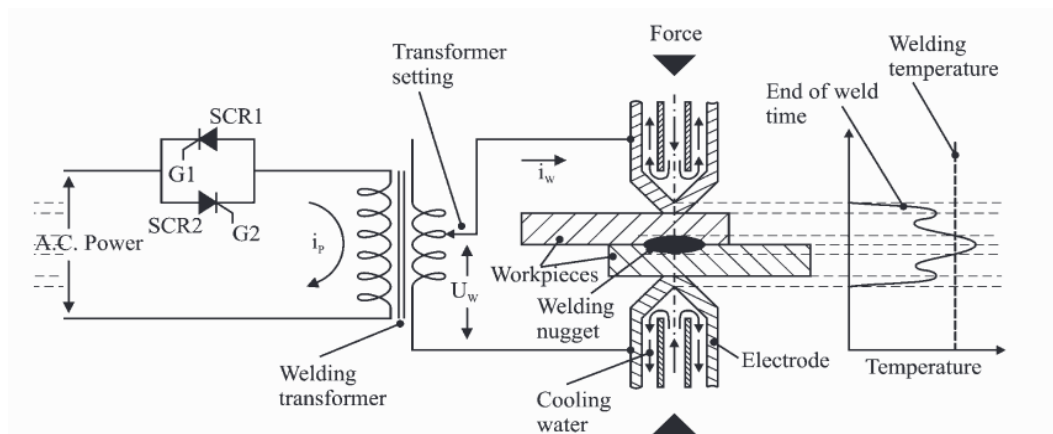


Figure 1. Schematic Representation of Resistance Spot Welding [2]

The critical parameters for RSW are nugget/button size, penetration, indentation, cracks (surface and internal), porosity/voids, sheet separation and surface appearance. The welding nugget formation originated from heat generation. The required heat is from deposition of layers between the electrodes is the source of the required heat. The size of the welding nugget determines the strength of the welding. In the case where other parameters remain constant, the size of the welding nugget increases proportionally with the welding time. It is shown in Figure 2 [2].
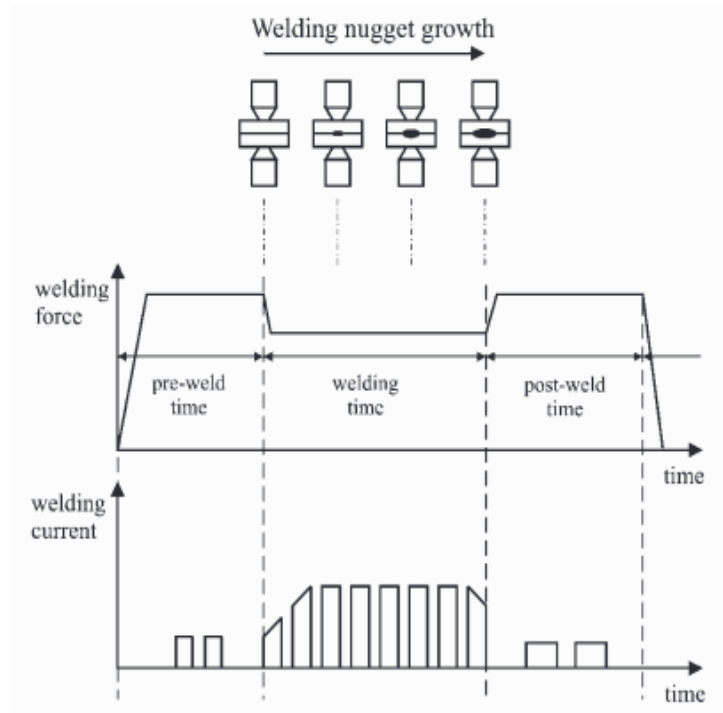


Figure 2. Growth of welding nugget versus welding time [2]

The diameter of the nugget is not the only parameter that defines the quality of the welding operation. The structural integrity of the weld and penetration affect the welding quality. Indeed, a weld is meant to contain all parts of a weldment, such as the heat-affected zone (HAZ), in addition to the nugget. The use of button diameter and nugget diameter is another case. A nugget and its size are usually determined by metallographic cross-sectioning. A nugget is subjected to measuring its width, not diameter, as shown in Figure 3 [3]. Moreover, HAZ is another parameter that determines the welding quality and should be at the optimum level.
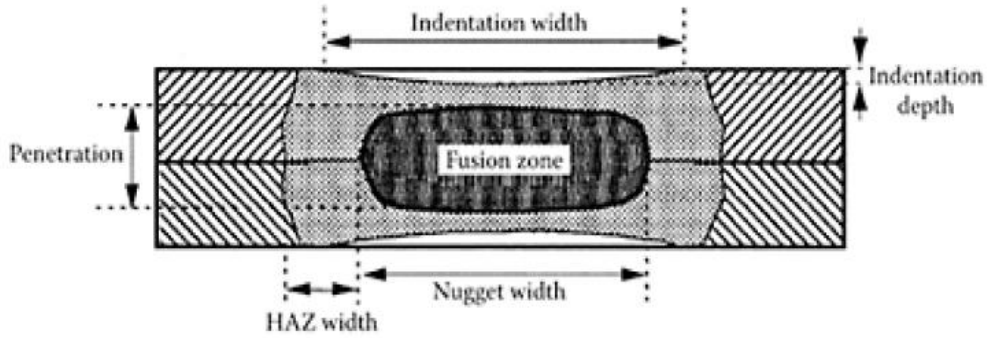
Figure 3. Metallographic Sectioning

The duration of the operation and the current generate the heat. Due to the high temperature on the surface between the welded parts, the alteration in the mechanical and metallurgical properties occurs in the welded region. This alteration affects the quality of the joint, and it should be at a minimum level with optimum operating conditions. Therefore, time, current, and electrode force are the essential parameters that determine mechanical properties.

The process parameters directly affect the strength of the resistance spot welding. The resistance spot welding strength is measured by destructive testing, such as hardness, impact and torsion, shear tensile and direct tensile tests [4].

## 2.2. The Problems in Al/Steel RSW

Since the mechanical, thermal, and metallurgical properties of aluminium and steel materials are different, welding these two materials is seen as problematic. The melting temperature of steel is higher than aluminium. As a result, it exhibits bad solidification behaviour in the HAZ of aluminium alloys. Due to differences, problems such as the formation of the aluminium oxide layer, deterioration, metallurgical precipitation, and defects may occur at the faying surface. Also, the solubility is very low in welding aluminium/steel. In parallel with this situation, a brittle intermetallic compound (IMC) layer may form at the faying surface [5].

4

Various methods are used to prevent the generation of the aluminium oxide layer. According to research conducted, zinc-coated steels are used to form the Al - Zn eutectic phase. The eutectic melt is gathered with the aluminium oxide layer [6].

Another issue is that there is an inequality in terms of the bulk resistance between aluminium and steel. As described in Figure 4, this situation centres the Joule heating towards the steel. The aluminium will begin to melt along the faying surface; it forms a weld nugget in the aluminium before any nugget formation [7]. Therefore, the liquid nugget formation is observed in aluminium.
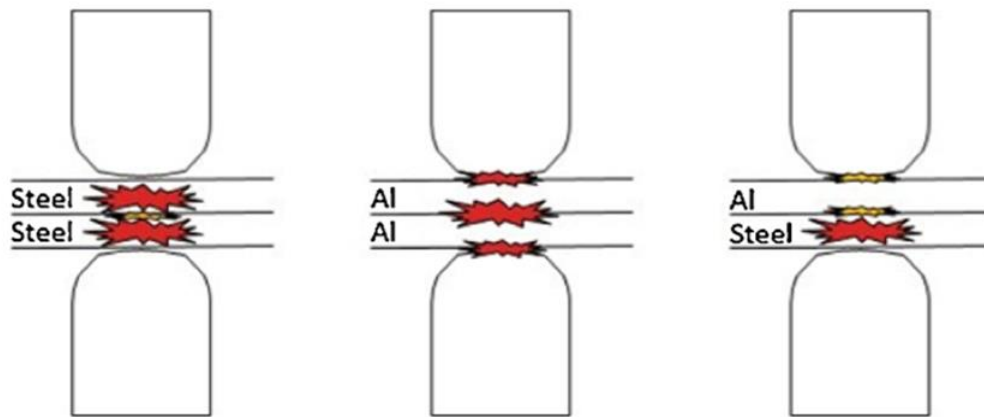


Figure 4.    Joule heating during resistance spot welding of various material combinations. Note the severe imbalance for Al/Steel stack-up [7]

The expansion of the IMC layer is also an essential condition in terms of strength. During the diffusion of iron into liquid aluminium, aluminium-rich IMC is formed as a result of the excessive saturation of the liquid in the iron. The expansion of the IMC layer is also a significant condition in terms of strength. During the diffusion of iron into liquid aluminium, aluminium-rich IMC is formed as a result of the excessive saturation of the liquid in the iron [8]. Miyamoto et al. (2009) studied the effect of the IMC thickness on the strength of the RSW area by using GI steel and 6xxx-series Al alloy. They used the eutectic reaction between aluminium and zinc in galvanized steel to obtain a sample with thin IMC thickness. To analyse the strength behaviour of samples with thin and thick IMC layer, joining test, tensile shear fatigue test, high/speed tensile test, and cyclic corrosion test was applied. This study is put down to the fact that there is an inverse proportion between IMC thickness and weld strength. In terms of the IMC layer, if it is

thick, then the strength of the joint is weak [9]. Figure 5 illustrates a cross-section which belongs to Al/Al, steel/steel and Al/steel RSW, and the formation of IMC.
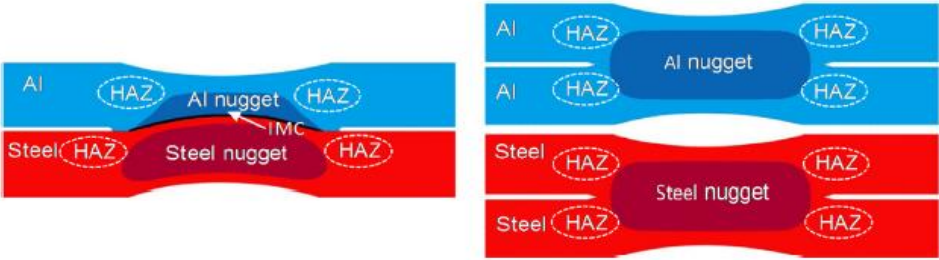


Figure 5. RSW of Al/Al, Steel/Steel and Al/Steel. [10]

## 2.3. Microstructure Analysis of RSW for Al/Steel

Microstructure analysis has been conducted in many research to investigate the joint between aluminum and steel. Some basic phenomena seen in the microstructural analysis are shown in Figures 6 and 7.
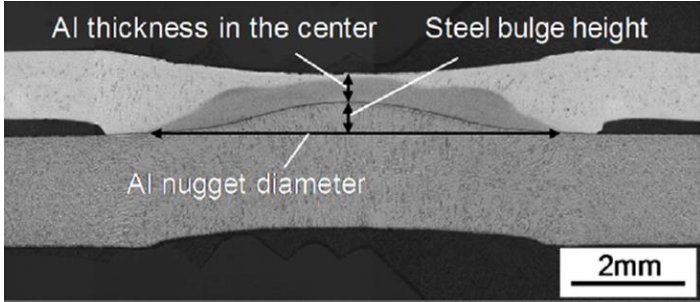


Figure 6. Definitions of different weld dimensions [10]
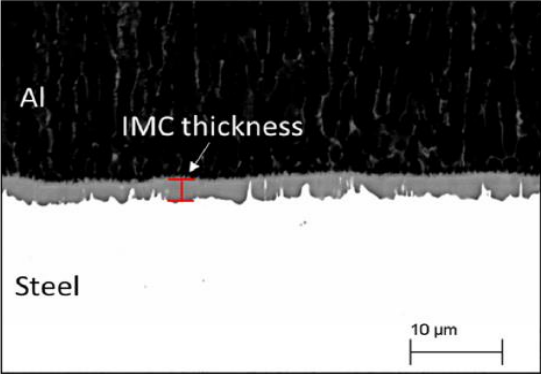


Figure 7. IMC thickness definition [10]

Qui et al. (2009) studied RSW between aluminum alloy A5052 to SPCC (Steel Plate Cold Commercial) and austenitic stainless steel SUS304 with a cover plate. The critical parameters in the study are as follows: welding current 6-12 kA, welding time 0.2 s, electrode force 1715 N, and pre-treatment with acetone. The microstructure of this study was made using a scanning electron microscope (SEM, JEOL JSM-6300, acceleration voltage:20Kv) and a transmission electron microscope (TEM; JEOL JEM-2000FX, acceleration voltage: 200Kv). In Figure 8, the welding current is 9 kA. According to Figure 8, the shape of the nugget is similar for both samples and includes blowholes. Porosity should be less than 40% of the nugget diameter not to affect the joint's strength, and in this case, the effect of the hole is low. Since the fusion zone (FZ) was not observed, it is concluded that the interface reaction takes place between molten aluminum and solid iron [11].
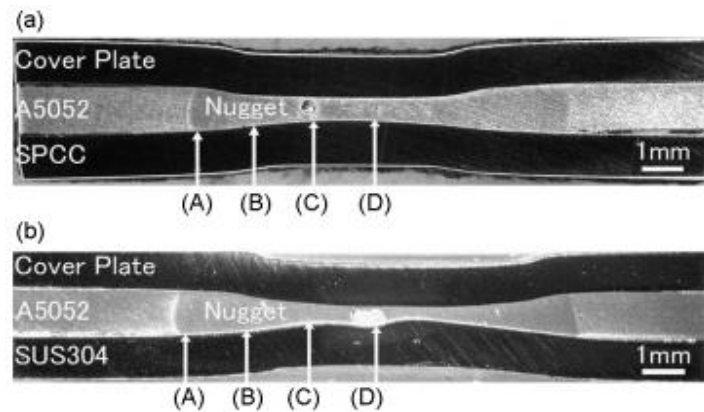


Figure 8.     Optical micrograph of the weld cross-section; (a) A5052/SPCC and (b) A5052/SUS304 [11]

In another study, RSW of A5052 aluminium alloy and DP600 steel was examined. RSW between A5052 and DP600 was performed by using different current values: 10.5-11.5-12.5-13.5 and 14.5 kA. The welding force is 3kN and welding time is 14 cycles. The limit value for thickness reduction is 15% by the American Welding Society. In this situation, the thickness reduction is 14% for 12.5KA. Furthermore, When Figure 9 is examined in terms of nugget size for 10.5 and 12.5 kA, it is observed that the size is proportional to the heat input, and the A5052 is greater in terms of the change in nugget size and shape (Chen et al.,2016) [12].
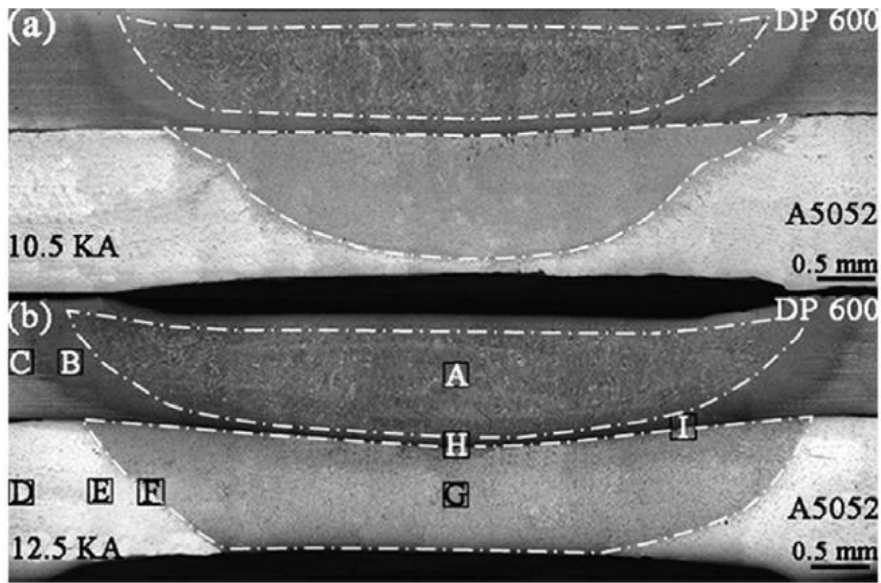
Figure 9. Optical micrograph images of A5052/DP 600 joints with different current parameters: (a) with current of 10.5 KA; (b) with current of 12.5 KA [12]

Figure 10 shows the steel side microstructure associated with Figure 9. The B region in Figure 9 and the b / e region in Figure 10 denote the HAZ. The C region in Figure 9 and the c / f region in Figure 10 represent the base metal (BM).
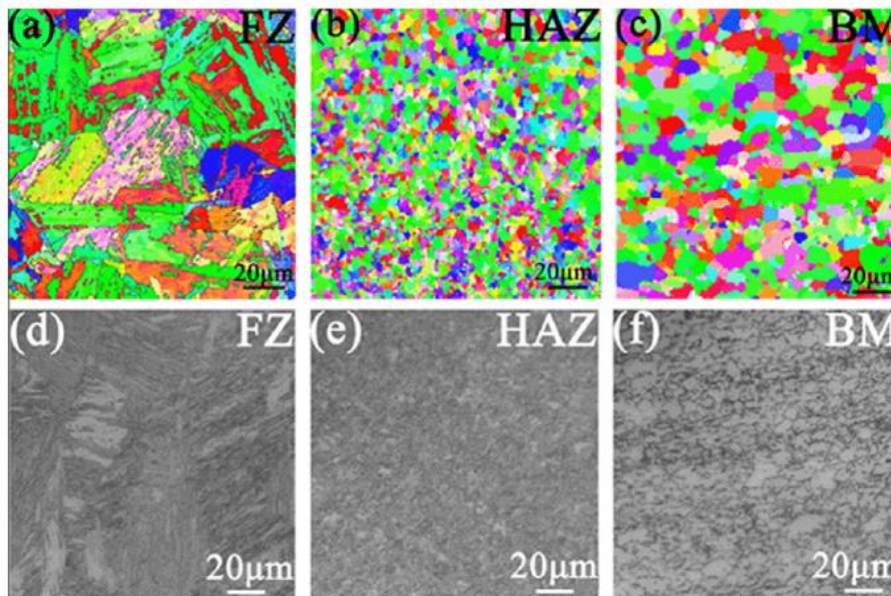


Figure 10.     Electron back-scattered diffraction (EBSD) profile of DP 600: (a), (d) FZ of DP 600 corresponds to region A in Fig. 7; (b), (e)HAZ of DP 600 corresponds to region B in Fig. 7; (c), (f)BM of DP 600 corresponds to region C [12]

## 2.4. Fracture Situations of RSW for Al/Steel

The most common types of fractures are ductile and brittle. Ductile fracture is accompanied by plastic deformation. It depends on the workpiece's elasticity, the acting force's loading speed, and the ambient temperature. In this type, the incoming energy is compensated with the plastic deformation, so it is desired. Another common type is a brittle fracture. There is little or no plastic deformation, so it is undesirable. The Lap Shear Tests, Cross Tension Tests, and Coach Peel Tests are experimental test types to observe the effects of failure mode.

RSW can generally break into two different types, interfacial and pullout failure. Interfacial failure occurs by way of crack propagation in the weld nugget. It is more common in small welds. Pullout failure arises when the weld nugget is completely pulled out from the workpiece by leaving a circular hole, and it is often observed in large welds. In Figure 11, interfacial and pullout failure are illustrated [13].
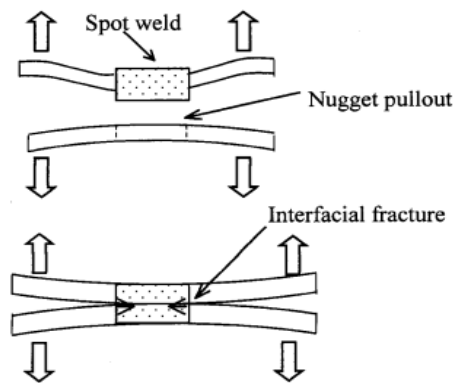


Figure 11. Nugget Pullout and Interfacial Fracture Representation [13]

Chen et al. (2016) researched the fracture mechanisms of Al/steel RSW. This study examined the RSW of aluminum alloy AA6022-T4 and hot-dipped galvanized low-carbon steel (HDGLCS). There are two sets of samples: one with a welding time of 200ms and welding currents of 13-14-15 kA; the second with a welding current of 13kA and welding time of 400-600-800ms. Determined fracture mechanisms and failure modes can be listed as semi-brittle or brittle fracture in the IMC layer, inter-surface fracture, ductile aluminum fusion zone (FZ) fracture, and ductile fracture in the aluminum HAZ. For the first set, there was a failure due to buttons or the thickness of aluminum left on steel, and

for the second set, samples failed without the remaining button and thickness. Figure 5 shows the results of the lap shear test conducted on the RSW of Al/steel. Button pullout failure originated from the strain localization in the aluminum HAZ, and the fracture occurred at the aluminum HAZ. The thickness failure occurred in the fore of the weld nugget at the faying surface. Interfacial failure is caused by the thick IMC layer [10].
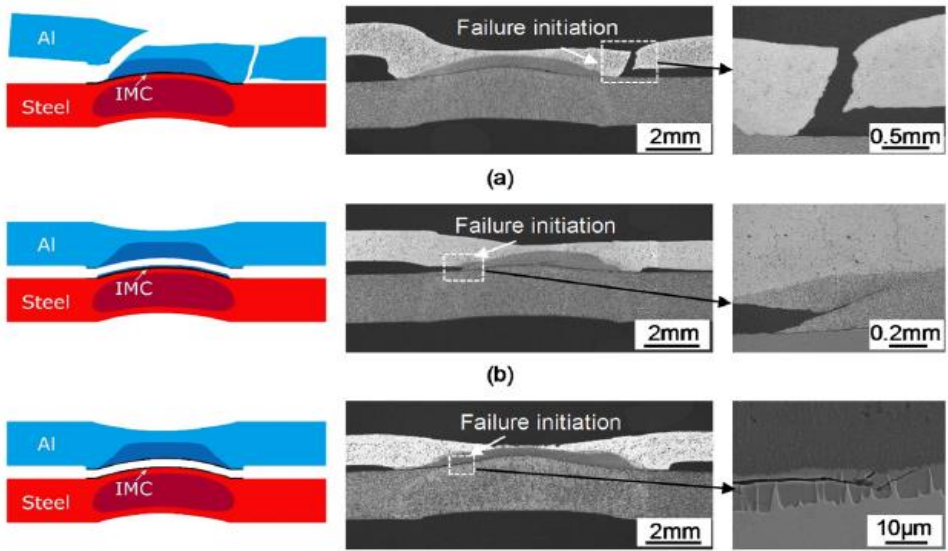


Figure 12.      Failure Types (a) Button pullout failure; (b) Thickness failure; (c) Interfacial failure [10]

Lu et al. (2019) demonstrated that welding current has a considerable impact on the failure modes of Al/Steel Ultrasonic+RSW by using different welding currents (varied from 12 to 17kA) with 3.56kN electrode force and 5 cycles (0.083s) welding time to samples. The fracture energy and nugget size increased directly proportional to the welding current. In this study, Shear fracture at Al/insert interface with current less than 13kA (Type 1), nugget pullout fracture from insert between 13.6-15.2 kA (Type 2), button pullout fracture from aluminum and interfacial fracture above 15.2 kA (Type 3) were observed. The different modes may arise due to nugget size, electrode indentation, the thickness of the IMC layer, and weld defects. These failure modes are represented in Figure 13 [14].
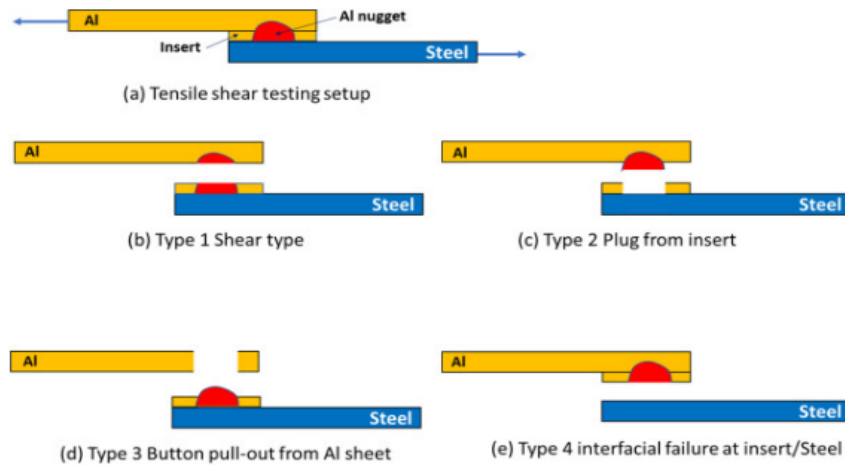
Figure 13. Representation of four different failure modes [14]

## 2.5. Fatigue Properties of RSW for Al/Steel

There are test methods to understand the failure behavior of specimens. Some of these are tensile-shear and coach-peel tests. The tensile-shear test helps to find out the ductility of the joint and the weld strength. The lap joint specimen is pulled with tension in the tensile-shear test. The coach peel test provides information about the nugget size and the weld strength. In Figure 14, the representation of tensile-shear and coach-peel tests are given.
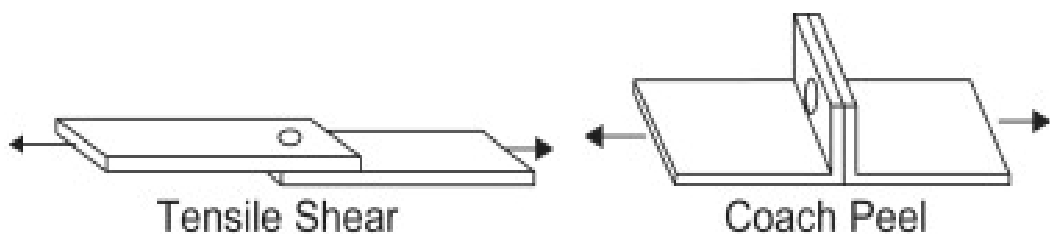


Figure 14. Representation of tensile-shear and coach peel test [15]

Rao et al. (2019) conducted a study on fatigue properties of RSW for aluminum AA6022-T4 and IF steel with 12.2 kA welding current, 3.1 kN welding force, and 1665 ms weld time by using tensile-shear and coach-peel test. They have compared Al / Al joining (3.1kN weld force, 24.1kA weld current, and 141 ms weld time) and Al / Steel joining. It is stated that the joint of Al/steel exhibited much higher fatigue life compared to similar Al/Al welded joints in the tensile-shear test. In addition, the tensile shear strength and fatigue life depend on the nugget size for the tensile-shear test. For the coach-peel test,

the nugget size does not affect these properties [16]. In figure 15, micrographs of the weld cross-section used in this study are given.
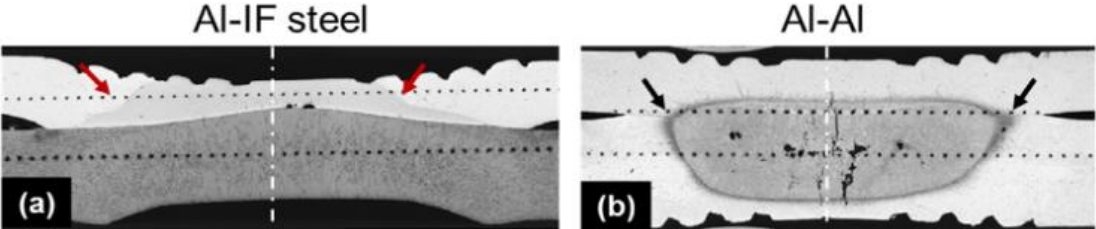


Figure 15. Micrograph of a) AA6022-T4 to IF steel, (b) AA6022-T4 to AA6022-T4[16]

Kang et al. (2015) studied load-controlled fatigue behavior and made microhardness measurements. They used RSW of 2mm thick AA5754 wrought sheet and 3mm thick Aural2 die casting sheet. For the load-controlled fatigue tests, a stress ratio of 0.1 with maximum load levels of 3483N, 2322N, 1744N, 1450N, and 1161N. It was concluded from the measurements that the microhardness of the weld nuggets was higher than the other parts of the weld. Microhardness results are shown in Figure 16 [17].
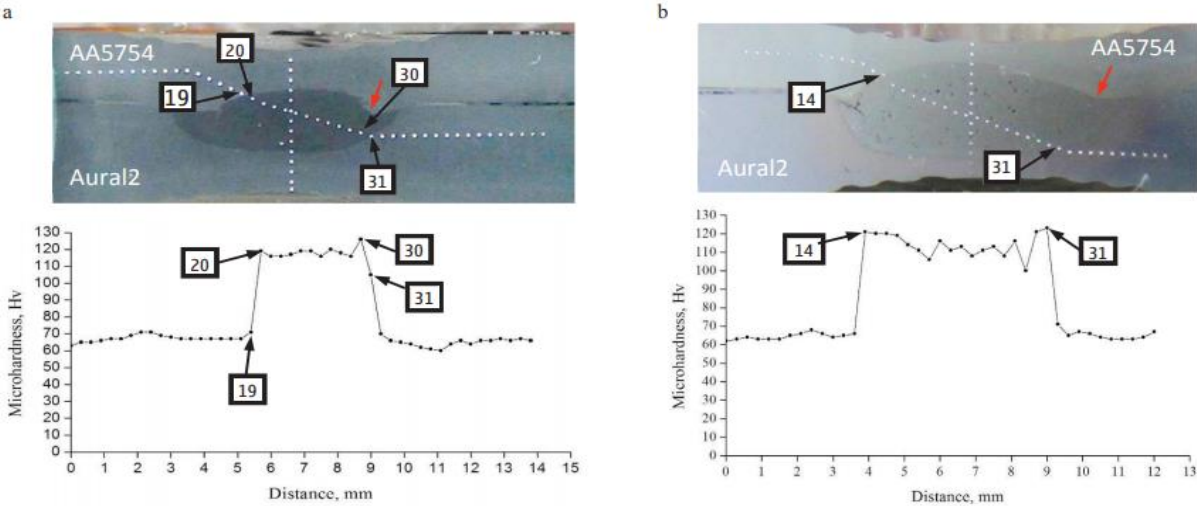


Figure 16.      Macrostructure and microhardness of AA5754 to Aural resistance spot welds (a) without adhesive and (b) with adhesive [17].

# 3. EXPERIMENTAL PROCEDURES

## 3.1. Specimen Properties

The material pair selected in the experimental study for resistance spot welding of different metals are MS1500 and EN AW-6061. The chemical composition of the MS 1500 and EN AW-6061 are given in Table 1 and Table 2, respectively.

Table 1. MS1500 Chemical Composition

| C [%] | Si [%] | Mn [%] | Al [%] | Ti [%] | Cr [%] | B [%] | Cu [%] |
|-------|--------|--------|--------|--------|--------|-------|--------|
| 0.271 | 0.207  | 0.77   | 0.268  | 0.036  | 0.023  | 0.010 | 0.116  |

Table 2. EN AW-6061 Chemical Composition

| Si [%] | Mg [%] | Fe [%] | Cu [%] | Mn [%] | Cr [%] | Zn [%] | Al [%] |
|--------|--------|--------|--------|--------|--------|--------|---------|
| 0.68   | 0.92   | 0.46   | 0.22   | 0.12   | 0.18   | 0.05   | balance |

For MS1500 and 6061, the mechanical properties are also listed in Tables 3 and 4.

Table 3. The mechanical properties for MS1500

| MS1500 | Yield Strength [MPa] | Ultimate Tensile Strength [MPa] | Elongation [%] |
|--------|----------------------|----------------------------------|----------------|
| Average | $1459.00 \pm 37.97$ | $1643.85 \pm 24.67$ | $5.47 \pm 0.81$ |

Table 4. The mechanical properties for EN AW-6061

| EN AW 6061 | Yield Strength [MPa] | Ultimate Tensile Strength [MPa] | Elongation [%] |
|------------|----------------------|----------------------------------|----------------|
| Average | $273.71 \pm 4.29$ | $332.32 \pm 3.46$ | $16.85 \pm 1.42$ |

In the experiments, MS1500 steel with dimensions of 45x105 mm and a thickness of 1.2 mm and EN AW-6061 aluminum material with the same measurements were employed. Sample surfaces were cleaned with acetone before welding. Figure 17 illustrates the

welded geometry of these two materials. To prevent bending and alignment problems that may occur during the tensile test, 40mm long and 1.2mm thick aluminum shims were welded to both ends of the samples with resistance spot welding.
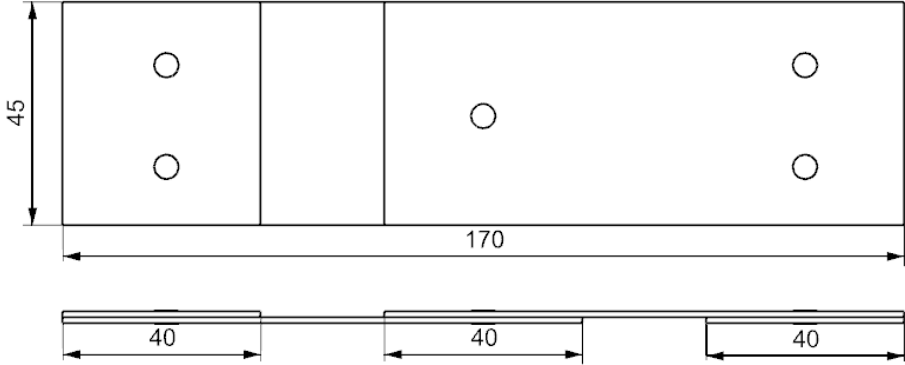


Figure 17. Sample Geometry

Copper chromium zirconium is the material utilized in the electrode geometry. There are three distinct electrode geometries employed. These are Ø6, Ø8 and R40. The effectiveness of steel-aluminum RSW was demonstrated to be influenced by electrode shape. Since aluminum and steel have different electrical and thermal properties, these different geometries have been tried to establish the heat balance between them. Figure 18 shows the geometry of the electrodes. Flat electrodes were used in every arrangement on the MS1500 side. Only the Al6061 side employed R40 electrodes.
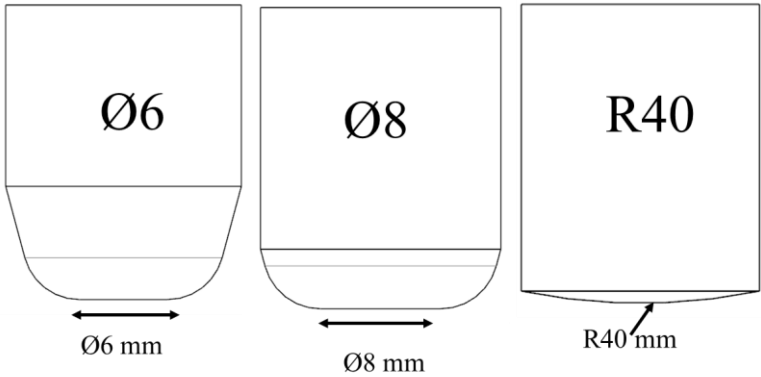


Figure 18. Electrode Geometries

Twelve combinations with different currents, electrode geometries, and welding times have been studied to obtain the best results. The electrode force was kept constant in these

combinations and taken as 3kN. Table 5 lists the sample combinations that were used in the testing. Seven samples were created for each combination, 84 in total, and the averages were used for the measured values.

Table 5. Sample Combinations

| Sample # | Current (kA) | Electrode Configuration | Electrode Force (kN) | Welding Tiime (cycle) |
|---|---|---|---|---|
| 1 | 11 | Ø6-Ø6 | 3 | 10 |
| 2 | 12 | Ø6-Ø6 | 3 | 10 |
| 3 | 13 | Ø6-Ø6 | 3 | 10 |
| 4 | 14 | Ø6-Ø6 | 3 | 10 |
| 5 | 11 | Ø8-R40 | 3 | 20 |
| 6 | 12 | Ø8-R40 | 3 | 20 |
| 7 | 13 | Ø8-R40 | 3 | 20 |
| 8 | 14 | Ø8-R40 | 3 | 20 |
| 9 | 11 | Ø6-R40 | 3 | 20 |
| 10 | 12 | Ø6-R40 | 3 | 20 |
| 11 | 13 | Ø6-R40 | 3 | 20 |
| 12 | 14 | Ø6-R40 | 3 | 20 |

## 3.2. Preparation of Specimens

There are two main types of welding machines used in RSW: pedestal type and robot type. While the pedestal type is highly rigid and robust, with high repeatability, its flexibility is low. In the robot type, flexibility is high, while repeatability is low. This study used a pedestal-type "UNIS UN-ALFA-10 380V Single Phase AC" equipment to weld. The machine has a 70 kVA power capacity and a CNC controller.

A specimen needs to be prepared in some ways to be seen under an optical microscope. First of all, it must be mounted onto a bakelite puck. It is then polished using increasingly fine sandpaper and a diamond paste. Finally, it must be etched.

For the specimens to get into the bakelite puck, they had to be divided into small parts, including the area of the nugget. The press brake machine was used to reduce the size of

the specimens. Since the samples formed at 11 kA were broken during the press brake machine operation, the microstructure analysis procedures were not applied to these samples.

Using epoxy resin and epoxy hardener at a ratio of 5:1, the cut specimen is mounted. After the bakelite was hardened, the part was machined using the "C11MSM" lathe until the nugget cross-sectional area was reached.

The specimens in which the bakelite process was completed were sanded with P400, P800, P1200, and P2500 sandpaper with a "METKON Forcipol 2V" device for microstructure analysis preparations. Then, polishing with 6µm and 1µm diamond solution was carried out with the same device.

Since there are two different materials, steel and aluminum, two other etching methods were used. Firstly, the steel is etched. While etching the steel, nital (95% alcohol, 5% nitric acid) solution was applied to the nugget area at a rate of 12% for 10 seconds.

After microstructure analyses were made on the sample, sanding and polishing processes were applied again, and the specimens were ready for aluminum etching. A mixture of 12 mL HCl, 30 mL HNO3, 1 mL HF, 12 g CrO3, and 40 mL water was used for the aluminum etch.

### 3.3. Experiments and Measurements

Tensile-shear test of 84 samples was conducted using the "UTEST Universal testing machine" at a constant speed of 10 mm/min according to ISO 14273. Etched surfaces were examined with a Nikon Eclipse LV150 optical microscope and the necessary images were recorded. Equipment to measure micro hardness was "FUTURE-TECH FM-700e." The tests were carried out according to the ISO 65071 standard; the test load was 500gf, and the dwell time was 15 seconds.

# 4. RESULTS AND DISCUSSION

The presented thesis has been summarized under five main headings; in this context, the results of the Tensile Shear Test, Nugget Properties, Hardness, Fracture, and Macrostructure/Microstructure analyses have been examined.

## 4.1. Tensile Shear Test

Aluminum and steel have different thermal and electrical properties. For instance, according to steel, aluminum has higher conductivity, expansion, and a lower melting point. Therefore, samples in different configurations were created to eliminate this situation and to observe its effects. Tensile tests were performed at 11-12-13-14 kA current values with Ø8-R40, Ø6-Ø6, and Ø6-R40 electrode configurations. Welding times for Ø8-R40, Ø6-Ø6, and Ø6-R40 are 20 cycles, 10 cycles, and 20 cycles, respectively. Force is 3kN for all cases. All test results regarding tensile strength are presented in Table 6 in Appendix 1. Additionally, Figure 19 was created to illustrate the average tensile strength and standard deviation values. Table 2, containing all the data related to fracture energy, is given in Appendix 2. Similarly, a diagram showing the mean fracture energy and standard deviation data is depicted in Figure 20. Force-displacement diagrams for 11-12-13-14 kA in all configurations based on these data are shown in Figure 21.

The influence of electrode configuration is obviously illustrated in these figures. The Ø8-R40 configuration has a lower tensile strength than the other two configurations. This is due to the fact that this configuration has a larger contact area between sheets than Ø6-Ø6 and Ø6-R40. As a result, the current density is decreased, which causes inadequate heating for welding. In addition, as the welding current increased, the welding strength decreased even more in the case of Ø8-R40, as the larger contact area resulted in lower pressure causing excessive expulsion.

The sample with the Ø6-R40 13 kA has the maximum tensile strength, fracture energy, and minimum standard deviation when the three configurations are evaluated. It has a

maximum of 4.63kN tensile strength. In the Ø6-R40 configuration, the contact areas of electrodes are different. R40 is for the aluminum side, and Ø6 is for the steel side. First contact occurs in a relatively limited area due to the electrode's curved tip for the aluminum side in this case, which leads to a higher current density and Joule heating. After then, a uniform heating zone can be expected as the contact area increases. The pressure caused by the molten aluminum can be suppressed by the electrode force pressure thanks to a 6mm flat geometry on the steel side. Therefore, compared to Ø8-R40, there was less expulsion.
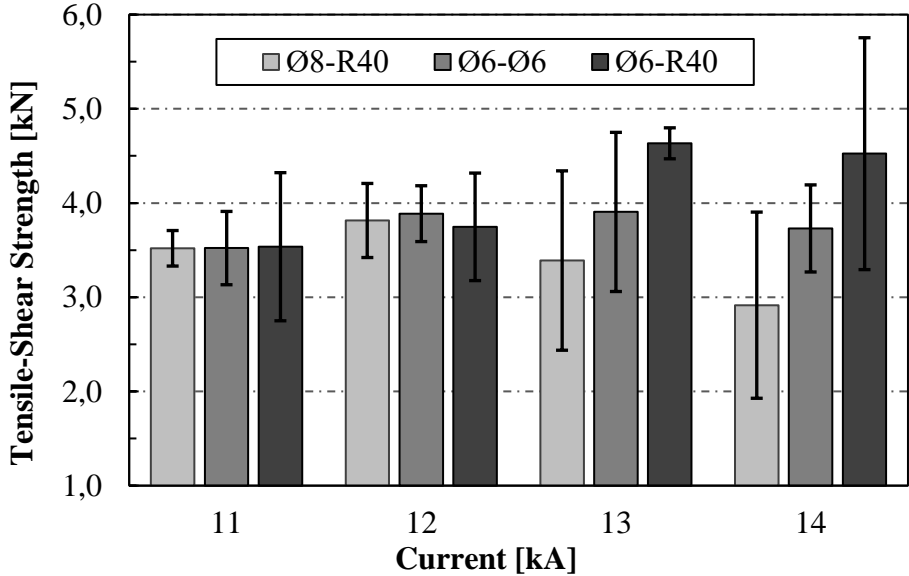


Figure 19. Tensile-Shear Strength/Current Diagram
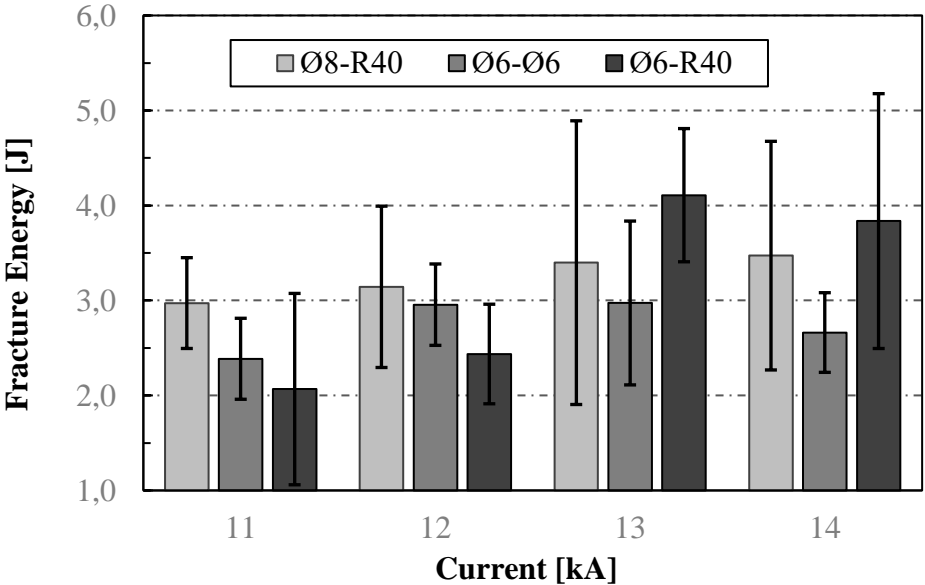
Figure 20. Fracture Energy/Current Diagram
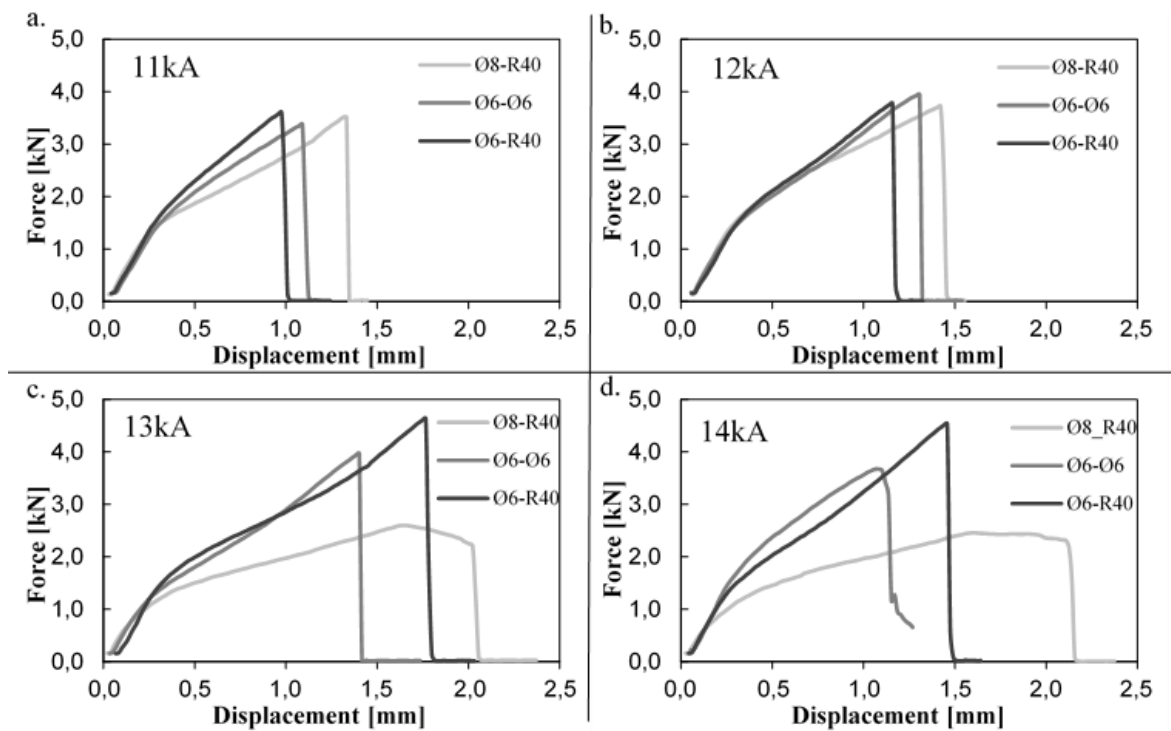


Figure 21. Force Displacement Graphs (a)11 kA; (b)12 kA; (c)13 kA; (d)14 kA

## 4.2. Nugget Properties

Three different electrode configurations were utilized. Flat electrodes (Ø6 and Ø8) were used for steel. On the aluminum side, R40 and Ø6 electrodes were used. The nugget surface of these electrode configurations at 11 kA-12 kA-13 kA and 14kA welding current are given in Figure 22. No external burn or expulsion was noticed on any of the surfaces in Figure 22.
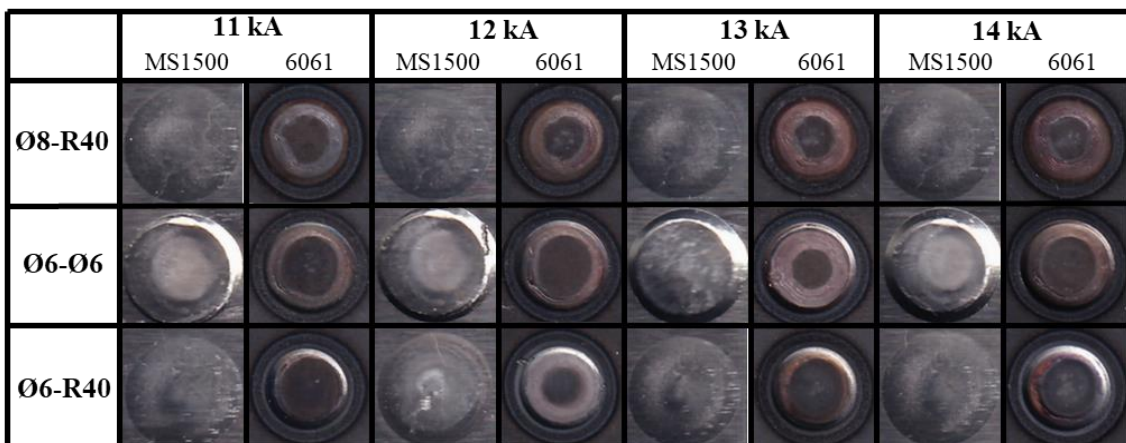


Figure 22.      Nugget surface of Ø8-R40, Ø6- Ø6 and Ø6-R40 electrode configuration

Figure 23 shows a nugget view taken from the fractured samples after the tensile test. In the Ø8-R40 and Ø6- Ø6 configurations, only 13kA welding current was examined since it was observed to be better than other current values in the tensile test results. However, the Ø6-R40 configuration gives better results than others. Images were taken at all current values.

As a result of current flow resistance, we convert the electrical energy into heat energy and increase the temperature. The aluminum expansion value is higher than steel; correspondingly, expulsion due to aluminum is more probable. Expulsions appearing on the steel material were formed by the contamination of aluminum material.

It is obvious that there is expulsion for all samples. When evaluated according to the current values of Ø6-R40, it can be said that the expulsion increases as the current increases. While there is a small expulsion for 11kA, we can observe that it gradually increases when we come to 14kA. The decrease in tensile test results observed after 13kA for the Ø6-R40 configuration is likely due to the expulsion at 14kA. In addition, when the images are examined in terms of the fracture mechanism, partial interfacial failure with expulsion is observed for all samples.

| | Ø8-R40 13kA | Ø6-Ø6 13kA | Ø6-R40 11kA | Ø6-R40 12kA | Ø6-R40 13kA | Ø6-R40 14kA |
|---|---|---|---|---|---|---|
| MS1500 | | | | | | |
| 6061 | | | | | | |
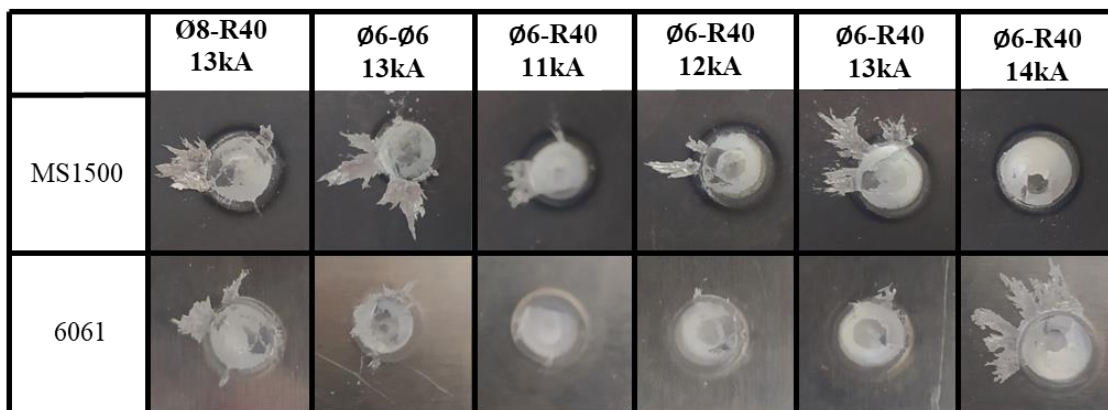
Figure 23. Nugget view taken from the fractured samples after the tensile test

The values in Figure 25 were formed using the positions in the schematic shown in Figure 24.
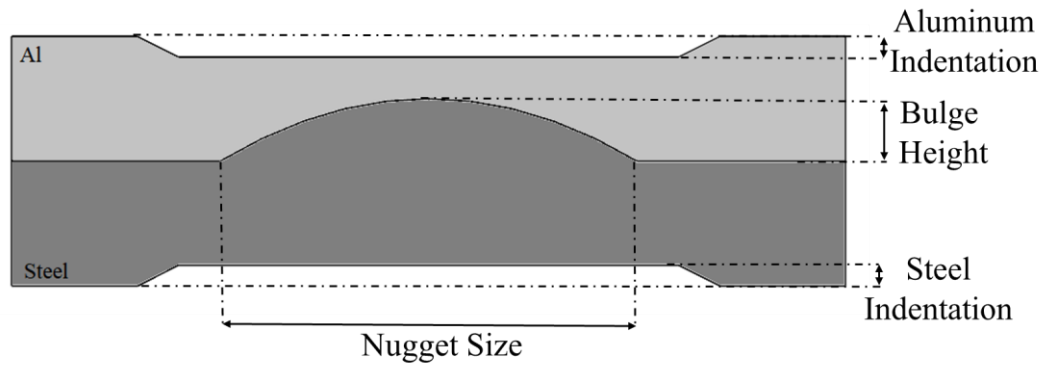
Figure 24. Schematic showing the details from which the measurements were taken

Nugget is the molten section of the joint. As is common knowledge, steel and aluminum materials have different thermal and electrical properties. These differences prevent the formation of a mutual nugget during steel-aluminum welding. Instead, a Fe-Al intermetallic layer is formed and provides the joint instead. In this study, the value specified as nugget size in Figure 25 gives the measure of this layer.

Nugget size is the most significant indicator of the strength, toughness, and characteristic of the mechanic of the joint. Nugget Sizes for the configuration of Ø8-R40, Ø6- Ø6 and Ø6-R40 in 13kA are depicted in Figure 25a. Comparing the three configurations at the same current, it was observed that the largest nugget size occurred in the Ø6-R40. This result is meaningful with the values encountered in the tensile test. It is stated that Ø6-R40 reached higher tensile-shear strength at 13kA than the others in Figure 19.

Bulge height is another critical parameter of resistance spot welding. Once more, Figure 25c examines three distinct configurations for 13kA (Ø8-R40, Ø6- Ø6, and Ø6-R40), while Figure 25d provides data for Ø6-R40 in 12-13-14kA. As in nugget size, in Ø8-R40, Ø6- Ø6, and Ø6-R40, Ø6-R40 has a larger bulge height ratio, and higher bulge height means higher strength. A more considerable bulge height is also observed at 13kA when the Ø6-R40 (12-13-14 kA) is evaluated independently.

An indentation is typically formed on each face when the electrodes compress the material. It is undesirable for the nugget to reach the material surface, as the material will

melt entirely and reduce electrode life. Therefore, less indentation is convenient. When analysing Figure 25e in terms of MS 1500, it can be said that Ø8-R40 has a lower indentation, but tensile strength is low in this configuration since there is not enough connection. Looking at the Ø6- Ø6 and Ø6-R40 at 13kA, the Ø6-R40 has a lower indentation.

Figure 25f shows the distribution of Ø6-R40 for MS1500 according to current values. A significant increase in indentation is observed at 14 kA. Figure 25g and Figure 25h compared indentation values for aluminum in different configurations and current values. Similar results have been seen.
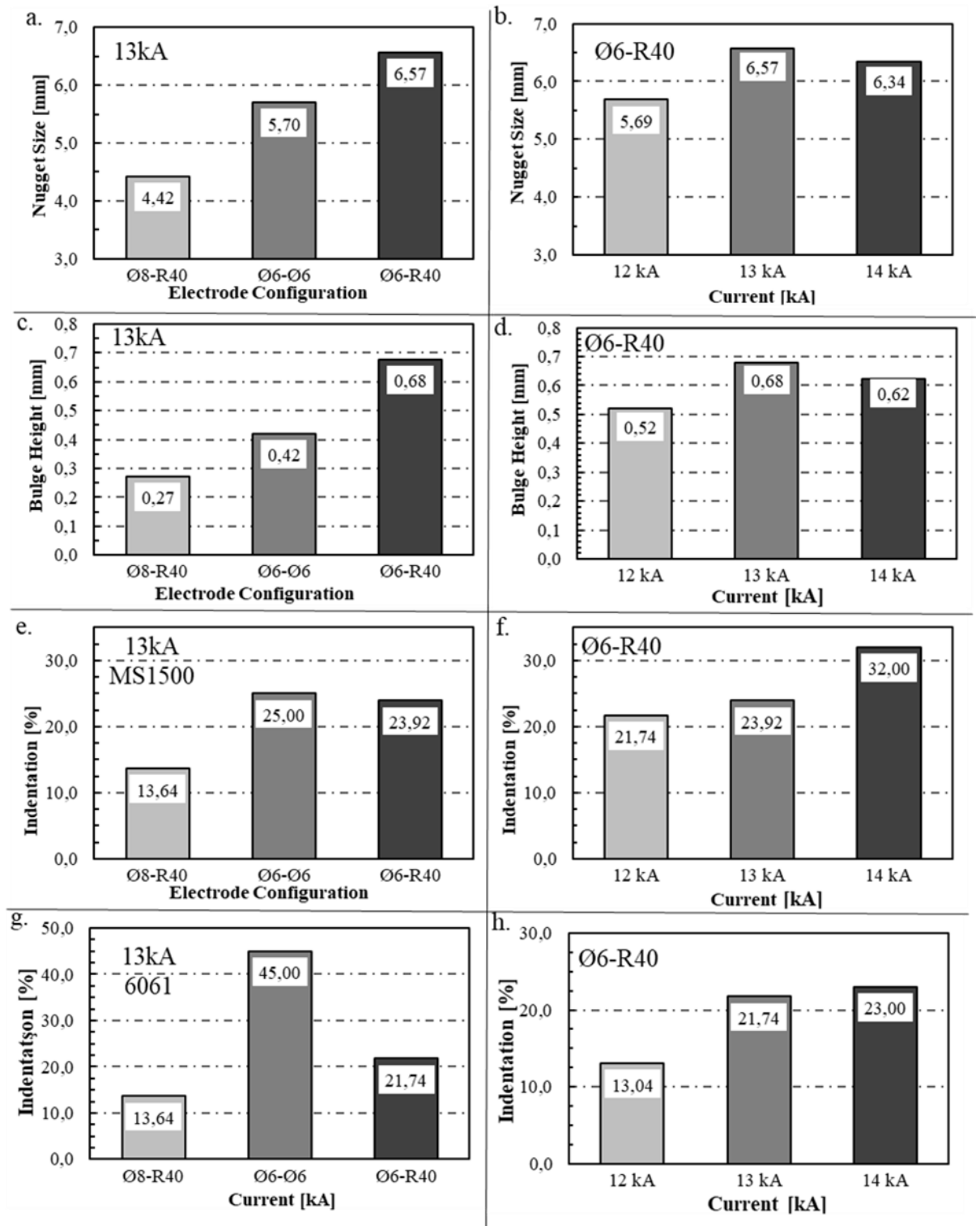
Figure 25.    Nugget Measurements a. Nugget Size for 13kA Ø8-R40, Ø6- Ø6 and Ø6-R40 b. Nugget Size for   12-13-14 kA Ø6-R40 c. Bulge Height for 13kA Ø8-R40 Ø6- Ø6 and Ø6-R40 d. Bulge Height for 12-13-14 kA Ø6-R40 e. MS1500 Indentation for 13kA Ø8-R40 Ø6- Ø6 and Ø6-R40 d. MS1500 Indentation 12-13-14 kA Ø6-R40 g. 6061 Indentation for 13kA Ø8-R40 Ø6- Ø6 and Ø6-R40 h. 6061 Indentation 12-13-14 kA Ø6-R40

## 4.3. Hardness

Figure 26 displays hardness profiles around the weld, including MS1500 and 6061. As a result of excessive martensite formation during rapid cooling following the welding process, hardness levels for steel showed a substantial rise. There was a considerable decrease in hardness values within the heat-affected zone (HAZ). This is because the martensite phase has re-crystallized in HAZ, and the deterioration of martensite structure in that region.

Figure 26b shows the MS1500 hardness graph of Ø8-R40 at 13kA. In this case, a distribution similar to the ones in the other graph did not occur, and the increase in hardness values remained low. This is due to sufficient melting is not achieved at Ø8-R40.

The hardness measurement graph of aluminum is given in Figure 26f. Hardness decreases were observed in the nugget region compared to the base metal. The change in grain size can be used to explain the decrease in hardness in the nugget zone. In addition, the natural aging structure in that region is deteriorating.
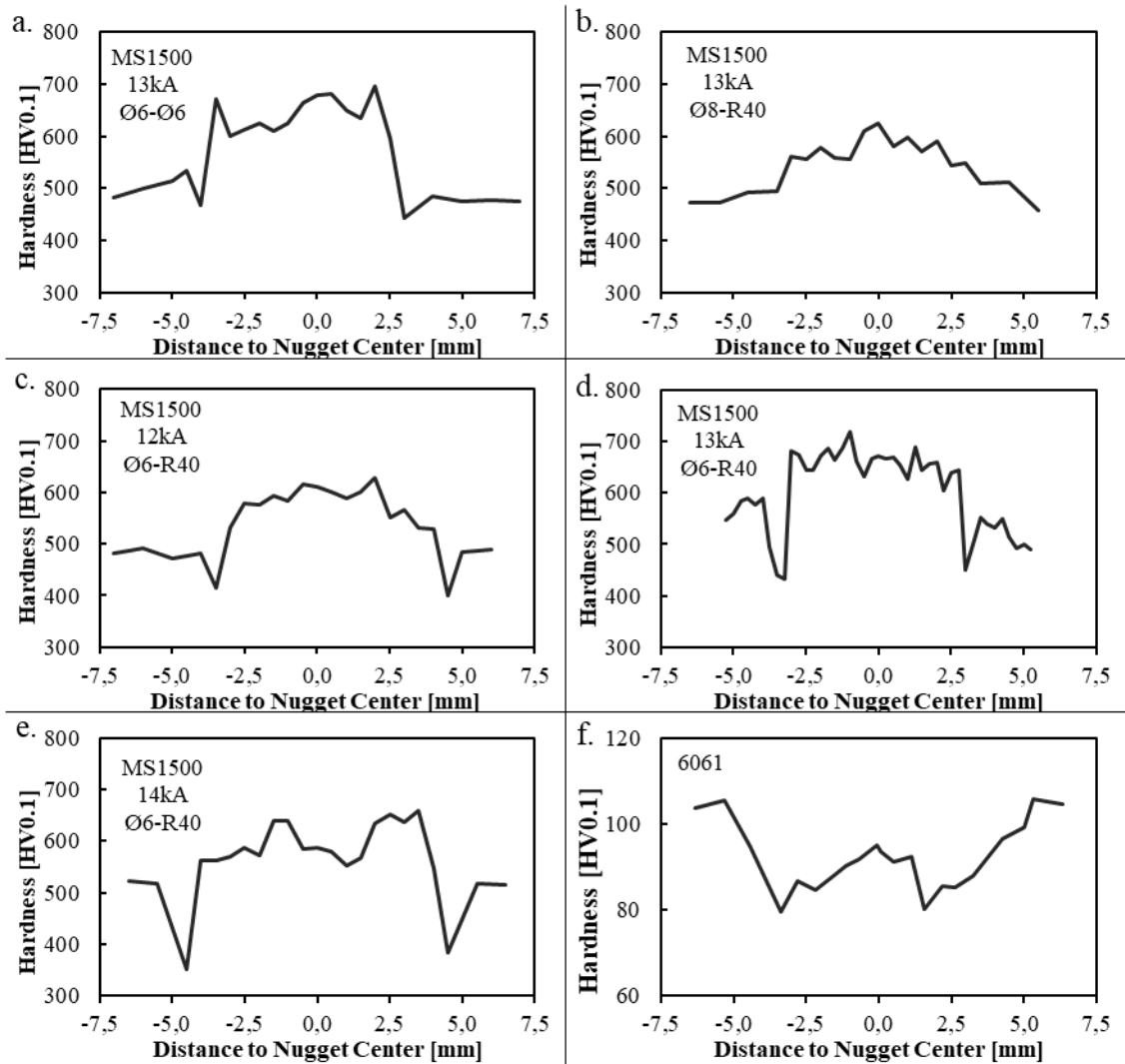
Figure 26.      Hardness characteristics a.MS1500 13kA Ø6- Ø6 b. MS1500 13kA Ø8-R40 c. MS1500 12kA Ø6-R40 d. MS1500 13kA Ø6-R40 e. MS1500 14kA Ø 6-R40 f. 6061

## 4.4. Fracture

There are fracture sample images in Figure 27, but the results are not of a quality to be analysed very well due to adhesive and resin residuals. However, when examined in Figure 23, given under "The Nugget Properties" title, it was observed that all fractures were in partial interfacial failure mode.
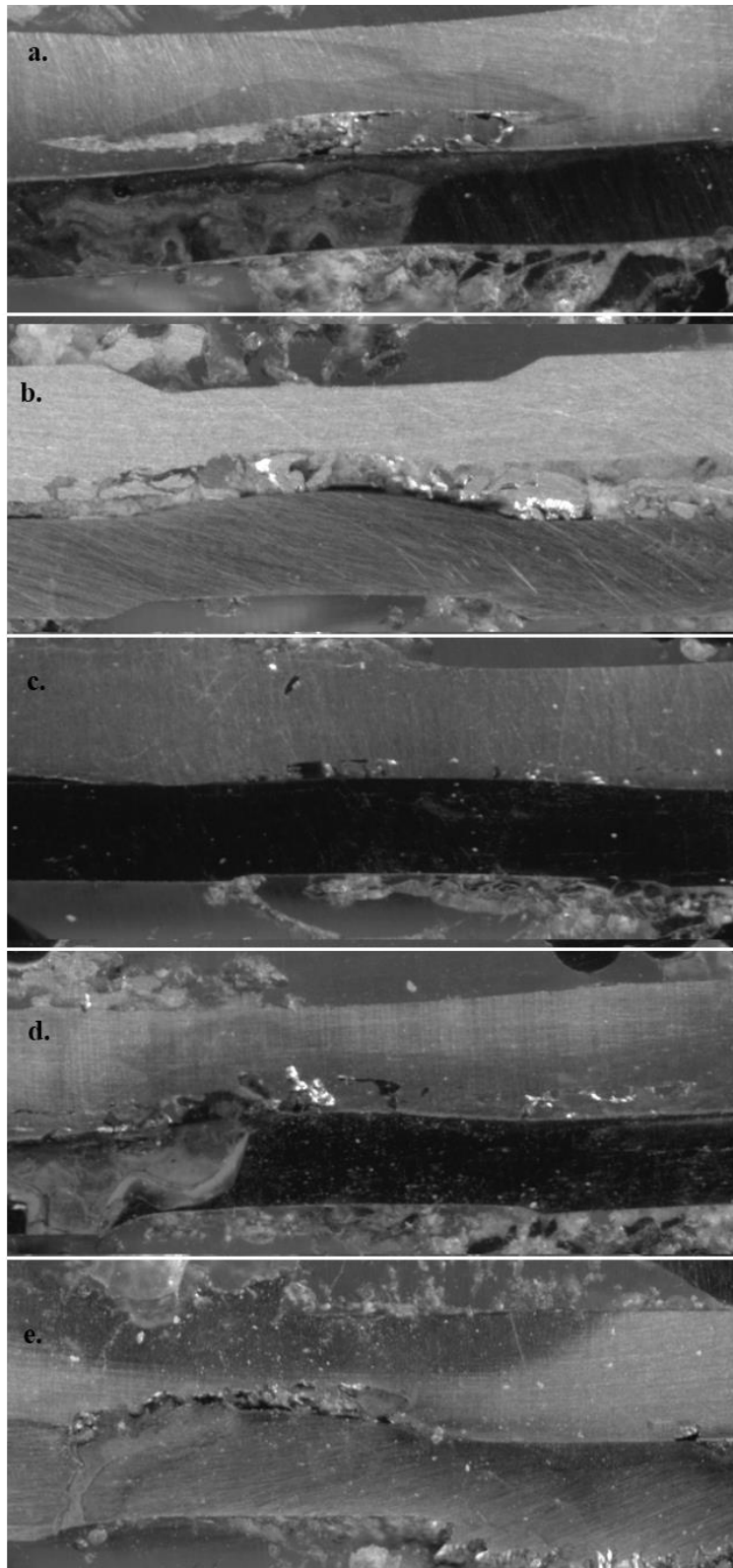
Figure 27.    Fracture samples a.13kA Ø8-R40 b. 13kA Ø6- Ø6 c. 12kA Ø6-R40 d. 13kA Ø6-R40 e. 14kA Ø6-R40

## 4.5. Macrostructure / Microstructure

The images showing the steel details of the etched joint of MS1500 are given in Figure 28. Figure 29 provides views of the etched aluminum that illustrate the aluminum's details.

The microstructure of the Ø6-R40 13kA weld can be examined in Figures 30 and 31 for the Ø6-R40 configuration in 13kA current. From the point of view of the MS1500, there is a heat-affected zone (HAZ) consisting of enlarged grains compared to the base metal in the region outside the nugget. Therefore, the reason for the decrease in the graphics (Figure 26) given under "the Hardness" title can be attributed to the grain structure in this region. Metal cannot be completely melted, hence the microstructure in HAZ is not martensite.

Steel has less martensite structure in the region close to the aluminum than in the interior away from the aluminum. This is because aluminum melted with a low melting point than steel and prevented martensite due to heat transfer in this region. The interior, however, showed significant martensite phase development. The base metal has a fine grained structure.

The initial microstructure is also seen in aluminum outside the melting zone. There is a highly oriented large grain structure in the nugget. Due to the heat transfer towards the junction point, the small grain region continues.

Figure 28.     MS1500 Etch a.13kA Ø8-R40 b. 13kA Ø6-Ø6 c. 12kA Ø6-R40 d. 13kA
                Ø6-R40 e. 14kA Ø6-R40
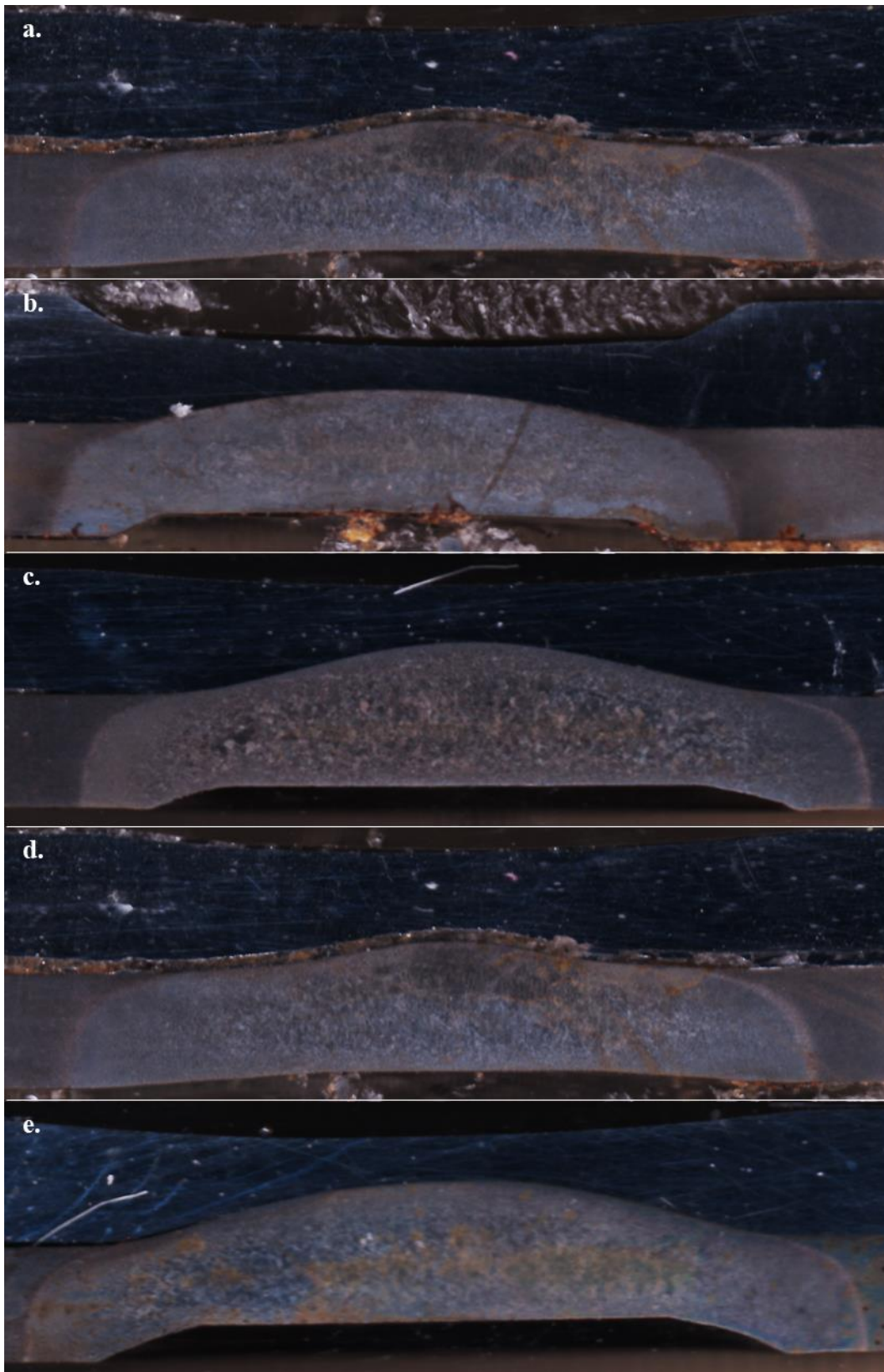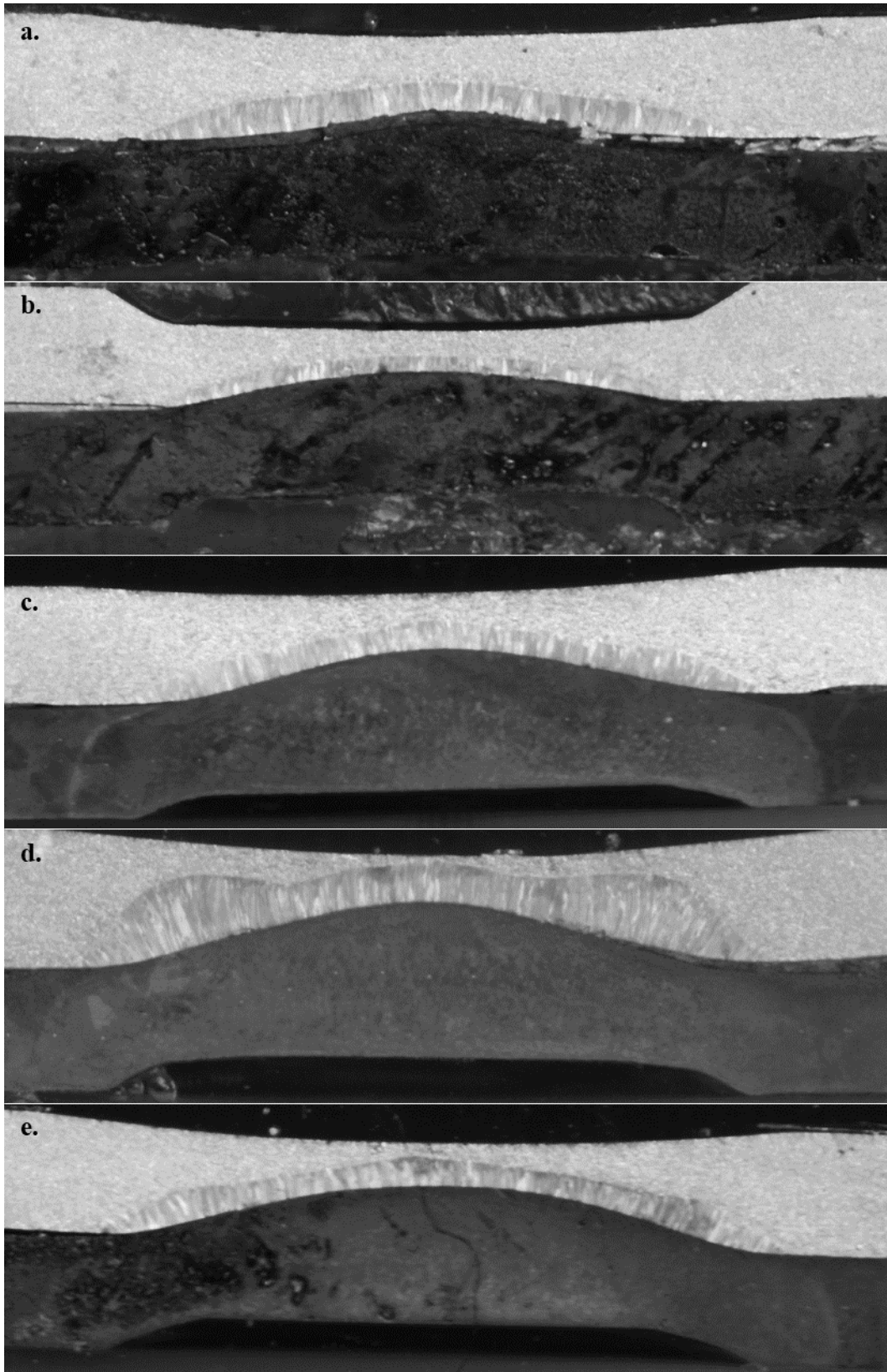
Figure 29.    Aluminum etch a.13kA Ø8-R40 b. 13kA Ø6- Ø6 c. 12kA Ø6-R40 d.
            13kA Ø6-R40 e. 14kA Ø6-R40
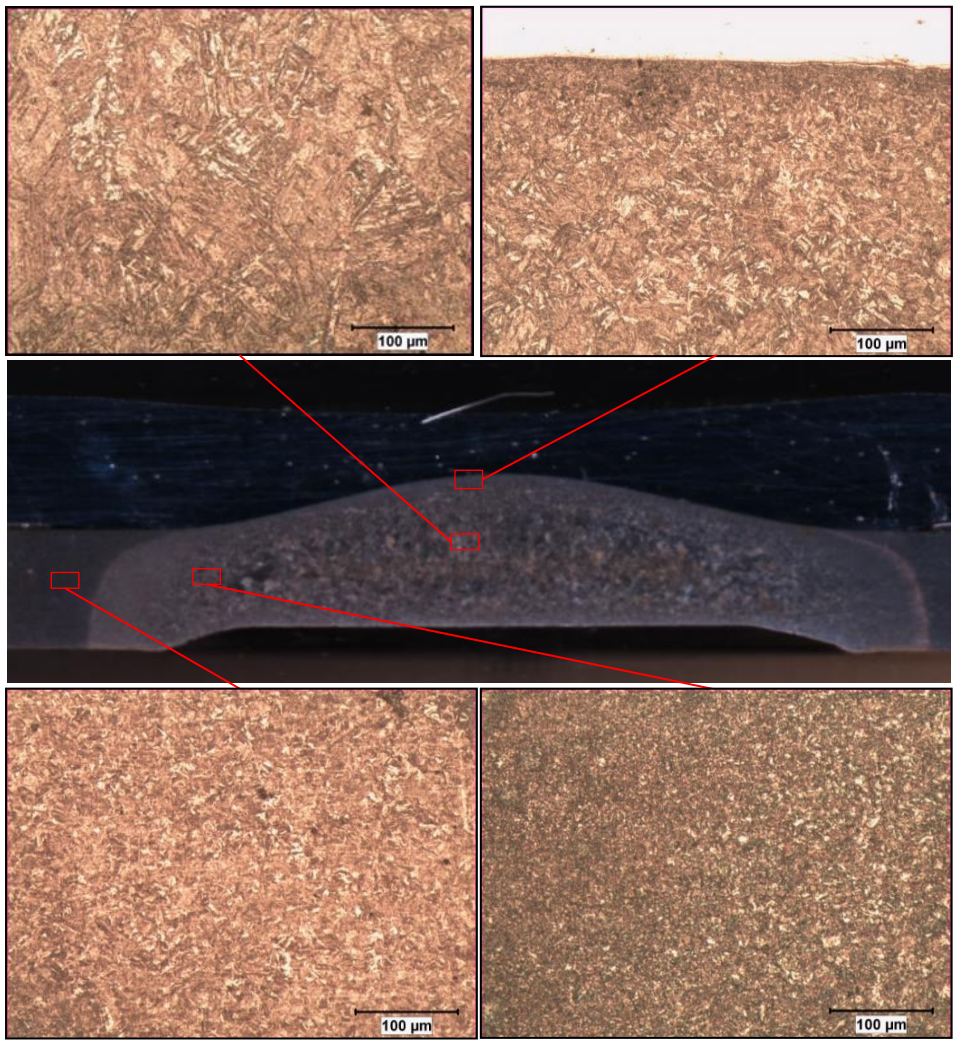
Figure 30. Microstructure analysis for 13kA Ø6-R40 configuration in MS1500 side
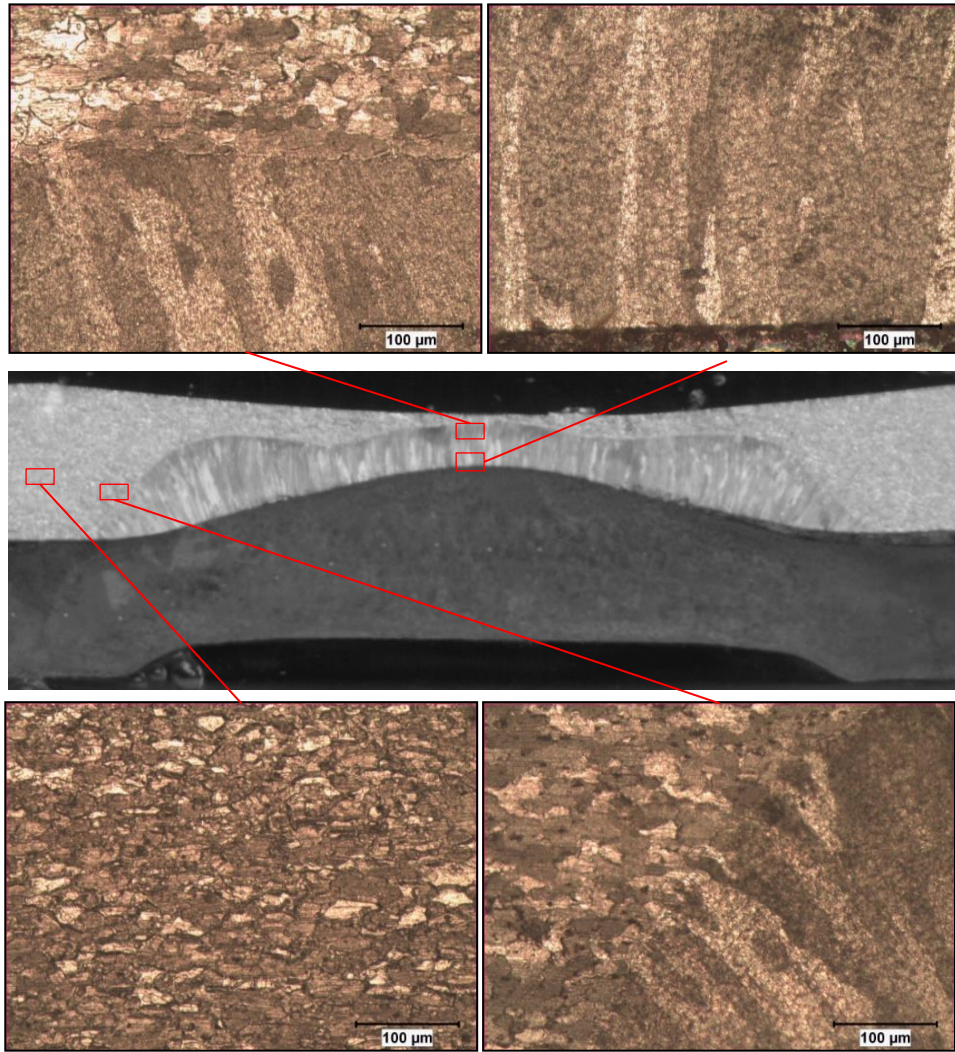
Figure 31. Microstructure analysis for 13kA Ø6-R40 configuration in 6061 side

# 5. SUMMARY AND CONCLUSION

In this study, it has been observed that 45x105mm, 1.2mm thick MS1500, and EN AW-6061 materials are welded to each other by the resistance spot welding method. The aim is to get optimum strength values. For this purpose, the tensile-shear test was performed, and the samples' micro hardness, microstructure, macrostructure, fracture, and nugget properties were examined. Electrode force was kept constant with 3kN. Current values were tested as 11-12-13-14 kA. Specimens were created in combinations of the Ø6, Ø8, and R40 electrode types. Welding time is used as 10 and 20 cycles.

According to the study's findings, the listed outcomes can be drawn:

1.  The sample with the highest tensile strength, lowest standard deviation, and highest fracture energy is the Ø6-R40 13 kA sample. Its tensile strength and fracture energy are 4.63 kN and xxx 4.11 J, respectively.

2.  In the Ø6-R40 configuration, the Ø6 electrode is on the steel side, and the R40 electrode is on the aluminum side. In this scenario, the curved electrode tip for the aluminum side causes first contact to occur in a relatively small region, resulting in a higher current density and Joule heating. This is why the Ø6-R40 design performs better.

3.  The Ø8-R40 configuration has the least tensile strength. Due to the increased contact area, the current density for the weld drops and insufficient heating occurs.

4.  For Ø6-Ø6 and Ø6-R40 configurations, an increase in tensile strength up to 13kA was observed, while a decrease was detected at 14kA. The reason for the drop in 14kA is expulsion. In Ø8-R40, the decrease started with 13 kA. Therefore, it can be said that it showed the expulsion effect before.

5. All samples showed partial interfacial failure with expulsion. As the current rises, the expulsion increases as well.

6. The largest nugget size was noted to occur in the Ø6-R40. The values found during the tensile test make this result valid. A larger bulge height is likewise seen at 13kA.

7. Steel's hardness levels significantly increased due to extensive martensite formation during rapid cooling after welding. Hardness parameters in the heat-affected zone (HAZ) were reduced significantly. The re-crystallization of the martensite phase and the degradation of the martensite structure in the HAZ are the causes of this.

8. In MS1500, the section outside the nugget has a heat-affected zone (HAZ) made up of grains that have expanded related to the base metal. The grain structure in this area could cause a decrease in hardness. Metal cannot be melted well all way. As a result, the HAZ microstructure is not martensite.

9. Steel has less martensite structure in the region close to the aluminum. Compared to steel, aluminum had a lower melting point. Due to heat transfer, the formation of martensite is lower in the region close to the aluminum than in the far region.

# 6. REFERENCES

[1]     H. M. Mallaradhya, V. Kumar M, R. Ranganatha, S. Darshan, and Lochan, "Resistance Spot Welding, A Review," *Int. J. Mech. Prod. Eng. Res. Dev.*, vol. 8, pp. 403–418, Apr. 2018, doi: 10.24247/ijmperdapr201846.

[2]     P. Podržaj, I. Polajnar, J. Diaci, and Z. Kariž, "Overview of resistance spot welding control," *https://doi.org/10.1179/174329308X283893*, vol. 13, no. 3, pp. 215–224, May 2013, doi: 10.1179/174329308X283893.

[3]     H. Zhang and J. Senkara, *Resistance welding: Fundamentals and applications, second edition*. 2011.

[4]     S. Shafee, B. B. Naik, and K. Sammaiah, "Resistance Spot Weld Quality Characteristics Improvement By Taguchi Method," *Mater. Today Proc.*, vol. 2, no. 4–5, pp. 2595–2604, 2015, doi: 10.1016/J.MATPR.2015.07.215.

[5]     L. H. Shah and M. Ishak, "Review of Research Progress on Aluminum–Steel Dissimilar Welding," *http://dx.doi.org/10.1080/10426914.2014.880461*, vol. 29, no. 8, pp. 928–933, Aug. 2014, doi: 10.1080/10426914.2014.880461.

[6]     M. P. Mubiayi and E. Akinlabi, "Friction Stir Welding of Dissimilar Materials between Aluminium Alloys and Copper - An Overview," *undefined*, 2013.

[7]     K. Martinsen, S. J. Hu, and B. E. Carlson, "Joining of dissimilar materials," *CIRP Ann.*, vol. 64, no. 2, pp. 679–699, Jan. 2015, doi: 10.1016/J.CIRP.2015.05.006.

[8]     M. Pouranvari, "Critical assessment 27: dissimilar resistance spot welding of aluminium/steel:           challenges           and           opportunities," *https://doi.org/10.1080/02670836.2017.1334310*, vol. 33, no. 15, pp. 1705–1712, Oct. 2017, doi: 10.1080/02670836.2017.1334310.

[9]     K. Miyamoto, S. Nakagawa, C. Sugi, H. Sakurai, and A. Hirose, "Dissimilar joining of aluminum alloy and steel by resistance spot welding," *SAE Tech. Pap.*, pp. 58–67, 2009, doi: 10.4271/2009-01-0034.

[10]   N. Chen, H. P. Wang, B. E. Carlson, D. R. Sigler, and M. Wang, "Fracture mechanisms of Al/steel resistance spot welds in lap shear test," *J. Mater. Process. Technol.*,     vol.     243,     pp.     347–354,     May     2017,     doi:

10.1016/J.JMATPROTEC.2016.12.015.

[11] R. Qiu, C. Iwamoto, and S. Satonaka, "Interfacial microstructure and strength of steel/aluminum alloy joints welded by resistance spot welding with cover plate," *J. Mater. Process. Technol.*, vol. 209, no. 8, pp. 4186–4193, Apr. 2009, doi: 10.1016/J.JMATPROTEC.2008.11.003.

[12] J. Chen, X. Yuan, Z. Hu, C. Sun, Y. Zhang, and Y. Zhang, "Microstructure and mechanical properties of resistance-spot-welded joints for A5052 aluminum alloy and DP 600 steel," *Mater. Charact.*, vol. 120, pp. 45–52, Oct. 2016, doi: 10.1016/J.MATCHAR.2016.08.015.

[13] Y. C.-S. and technology of welding and joining and undefined 2003, "Failure mode of spot welds: interfacial versus pullout," *me.sc.edu*, Accessed: Oct. 29, 2022. [Online]. Available: http://www.me.sc.edu/fs/pdf/stwj paper published.pdf.

[14] Y. Lu, E. Mayton, H. Song, M. Kimchi, and W. Zhang, "Dissimilar metal joining of aluminum to steel by ultrasonic plus resistance spot welding - Microstructure and mechanical properties," *Mater. Des.*, vol. 165, p. 107585, Mar. 2019, doi: 10.1016/J.MATDES.2019.107585.

[15] Y.-L. Lee, M. E. Barkey, and H.-T. Kang, "Metal fatigue analysis handbook : practical problem-solving techniques for computer-aided engineering," 2011.

[16] H. M. Rao, J. Kang, L. Shi, D. R. Sigler, and B. E. Carlson, "Effect of specimen configuration on fatigue properties of dissimilar aluminum to steel resistance spot welds," *undefined*, vol. 116, pp. 13–21, Nov. 2018, doi: 10.1016/J.IJFATIGUE.2018.06.009.

[17] J. Kang, Y. Chen, D. Sigler, B. Carlson, and D. S. Wilkinson, "Fatigue Behavior of Dissimilar Aluminum Alloy Spot Welds," *Procedia Eng.*, vol. 114, pp. 149–156, 2015, doi: 10.1016/J.PROENG.2015.08.053.

# APPENDIX

**APPENDIX 1 – Table 6**

Table 6. The average tensile strength formed by values taken from 7 samples

| Electrode Force (kN) | 3 | 3 | 3 | 3 | 3 | 3 | 3 | 3 | 3 | 3 | 3 | 3 |
|---|---|---|---|---|---|---|---|---|---|---|---|---|
| Time (cycle) | 20 | 20 | 20 | 20 | 10 | 10 | 10 | 10 | 20 | 20 | 20 | 20 |
| Electrode | 8-R40 | 8-R40 | 8-R40 | 8-R40 | 6-6 | 6-6 | 6-6 | 6-6 | 6-R40 | 6-R40 | 6-R40 | 6-R40 |
| Current (kA) | 11 | 12 | 13 | 14 | 11 | 12 | 13 | 14 | 11 | 12 | 13 | 14 |
| Sample-1 (kN) | 3.88 | 3.36 | 2.32 | 2.46 | 4.14 | 4.27 | 4.69 | 3.31 | 3.15 | 3.12 | 4.91 | 2.48 |
| Sample-2 (kN) | 3.52 | 3.34 | 3.82 | 3.92 | 2.89 | 4.21 | 3.24 | 4.29 | 3.19 | 3.81 | 4.58 | 4.79 |
| Sample-3 (kN) | 3.59 | 3.90 | 4.48 | 3.92 | 3.70 | 3.62 | 2.89 | 3.50 | 3.78 | 3.82 | 4.64 | 5.17 |
| Sample-4 (kN) | 3.88 | 4.13 | 4.12 | 2.02 | 3.35 | 3.95 | 4.25 | 4.06 | 4.84 | 4.52 | 4.87 | 4.79 |
| Sample-5 (kN) | 3.78 | 3.73 | 4.31 | 4.34 | 3.73 | 3.49 | 4.58 | 3.38 | 3.46 | 3.79 | 3.80 | 4.54 |
| Sample-6 (kN) | 2.64 | 4.21 | 2.08 | 1.62 | 3.38 | 3.72 | 3.72 | 3.89 | 2.73 | 3.56 | 4.63 | 4.70 |
| Sample-7 (kN) | 3.36 | 4.03 | 2.60 | 2.14 | 3.46 | 3.95 | 3.97 | 3.68 | 3.61 | 3.61 | 5.01 | 5.20 |
| **Average TS (kN)** | 3.52 | 3.81 | 3.39 | 2.92 | 3.52 | 3.89 | 3.91 | 3.73 | 3.54 | 3.75 | 4.63 | 4.52 |
| **Standard Deviation** | 0.19 | 0.39 | 0.95 | 0.99 | 0.39 | 0.30 | 0.84 | 0.46 | 0.79 | 0.57 | 0.16 | 1.23 |

**APPENDIX 2 – Table 7**

Table 7.The average fracture energy formed by values taken from 7 samples

| Electrode Force (kN) | 3 | 3 | 3 | 3 | 3 | 3 | 3 | 3 | 3 | 3 | 3 | 3 |
|---|---|---|---|---|---|---|---|---|---|---|---|---|
| Time (cycle) | 20 | 20 | 20 | 20 | 10 | 10 | 10 | 10 | 20 | 20 | 20 | 20 |
| Electrode | 8-R40 | 8-R40 | 8-R40 | 8-R40 | 6_6 | 6_6 | 6_6 | 6_6 | 6-R40 | 6-R40 | 6-R40 | 6-R40 |
| Current (kA) | 11 | 12 | 13 | 14 | 11 | 12 | 13 | 14 | 11 | 12 | 13 | 14 |
| Sample-1 (J) | 3.57 | 2.04 | 1.61 | 2.67 | 2.51 | 3.38 | 3.88 | 2.88 | 1.45 | 1.58 | 4.08 | 1.03 |
| Sample-2 (J) | 2.71 | 2.01 | 2.92 | 5.28 | 1.57 | 3.52 | 1.70 | 3.26 | 1.53 | 2.30 | 3.83 | 4.31 |
| Sample-3 (J) | 3.06 | 3.16 | 4.35 | 3.96 | 2.84 | 2.83 | 1.95 | 2.22 | 2.25 | 2.89 | 4.55 | 4.36 |
| Sample-4 (J) | 3.37 | 3.39 | 6.08 | 2.01 | 2.29 | 3.13 | 3.07 | 2.91 | 4.06 | 3.20 | 5.05 | 3.79 |
| Sample-5 (J) | 3.30 | 3.29 | 3.77 | 4.34 | 2.63 | 2.37 | 3.93 | 2.13 | 2.25 | 2.49 | 3.02 | 3.67 |
| Sample-6 (J) | 2.44 | 3.87 | 2.20 | 2.24 | 2.18 | 2.50 | 3.21 | 2.84 | 0.90 | 2.49 | 3.57 | 4.43 |
| Sample-7 (J) | 2.35 | 4.24 | 2.86 | 3.82 | 2.68 | 2.96 | 3.08 | 2.39 | 2.03 | 2.11 | 4.66 | 5.26 |
| **Average Energy (J)** | 2.97 | 3.14 | 3.40 | 3.47 | 2.39 | 2.96 | 2.97 | 2.66 | 2.07 | 2.44 | 4.11 | 3.84 |
| **Standard Deviation** | 0.48 | 0.85 | 1.49 | 1.20 | 0.43 | 0.43 | 0.86 | 0.42 | 1.01 | 0.52 | 0.70 | 1.34 |